

Effect of Non-Metallic Inclusions on Bending Fatigue Performance in High Strength 4140 Steel

Michael E. Burnett, Peter C. Glaws and Daniel K. Gynther

The statements and opinions contained herein are those of the author and should not be construed as an official action or opinion of the American Gear Manufacturers Association.

Introduction

The fatigue performance of three sets of quench and tempered 4140 steel samples, representing three distinctly different inclusion populations—low oxygen/low sulfur, high oxygen/low sulfur and low oxygen/high sulfur—were evaluated through a series of various bending fatigue tests. Three different bending fatigue tests with differing stress ratios were employed, including: rotating bending (-1); single-tooth bending (0.1); and modified Bruggen (0.1). The inclusion populations for each of the three steel sample sets were characterized using both a SEM-based image analysis system, primarily for the micro-inclusions, and a high-resolution UT system for the macro inclusions. All three sample sets were evaluated using both longitudinal and transverse specimens in all the bending fatigue tests. The transverse samples displayed significantly lower fatigue performance (typically ~50% lower fatigue strength values) than the longitudinal samples. Furthermore, the high-sulfur sample set clearly had the lowest performance in the transverse orientation. While there was more scatter with the data on the longitudinal samples, the high-oxygen sample set had a lower fatigue strength and a higher percentage of the failures initiating at subsurface oxides than the other two sample sets.

In general terms, non-metallic inclusions can have a measureable impact on many steel properties. Perhaps most significant is the effect on fatigue

properties. Previous studies, compiled and reviewed by Murakami (Ref. 1), have demonstrated that a linear correlation exists between bending and axial fatigue strength and the ultimate tensile strength (UTS) in low- and medium-strength steels. However, in high-strength steels ($H_v > 400$) (*Note: a strong correlation exists between UTS and hardness in these steels. Accordingly, Vickers hardness is often used as a proxy for UTS in many fatigue studies.*) the linear correlation fails, and there is significant scatter in the measured fatigue strength (Refs. 1-4). This deviation from linearity often has been attributed to the presence of non-metallic inclusions. In many cases, the fatigue origin, often clearly identifiable by a “fish-eye” pattern, is observed to be subsurface with a non-metallic inclusion located at the center (Fig. 1). The effect of individual inclusions on the fatigue performance, and in particular the fatigue strength, of a given steel will

be a function of the inclusion type, size, morphology, and location/orientation with respect to the principle stresses from the applied cyclical load. The properties of the inclusion/matrix interface also can play a significant role.

The effect of non-metallic inclusions, especially oxides, on fatigue performance in bearings, gears, and other high-cyclic load applications has long been a subject of study. Our understanding of the relationship between inclusion content and fatigue performance has been enhanced with the continued improvement of tools and methods employed in steel cleanliness measurement.

In the current study, single-gear tooth bending (STB), Bruggen beam-type bending and rotating bending fatigue (RBF) tests were conducted on three sets of quenched and tempered 4140 steel samples, representing three distinctly different inclusion populations—low oxygen/low sulfur, high oxygen/low sulfur, and low oxygen/high sulfur. The inclusion populations for the three sample sets were characterized using both an advanced SEM-based image analysis system, primarily for the micro-inclusions, and a high-resolution UT system for the macro-inclusions.

Experimental

Materials. Three sets of 4140 steel samples of varying sulfur and total oxygen contents were employed in this study. Group A was low oxygen/low sulfur; Group B was high oxygen/low sulfur; and Group C was low oxygen/high sulfur. The compositions of each group are provided in Table 1.

The inclusion population of each sample group was fully characterized by SEM-based image analysis and

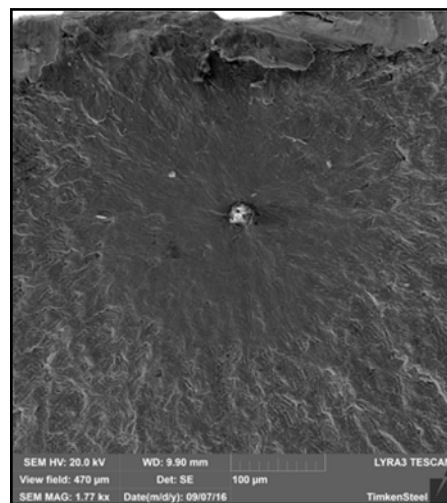


Figure 1 SEM image of subsurface fatigue initiation site showing common fish-eye pattern with globular oxide inclusion at the center.

high-resolution ultrasonic testing. The key metrics for the oxide inclusion populations were total oxide area; area of large oxides; oxide stringer length; and area (all normalized by sample inspected area). Key metrics for sulfide inclusions included total sulfide area and area of large sulfides. Statistics of extreme values (SEV) analysis was also performed to provide additional information about the inclusion populations. To provide a description of the oxide and sulfide populations of the three sample groups in terms of an industry standard, the data from the SEM image analysis was configured to generate DIN 50602 values (K0 – K4). The measured values for inclusion population metrics are provided in Tables 2A and 2B. The respective DIN 50602 oxide (OG+OA) and sulfide (SS) plots are shown (Figs. 2A and 2B).

The inclusion evaluation showed that the relationship between total oxide area and oxygen content of the steel was approximately linear. Group B had about twice the total oxygen content, as well as about twice the total oxide area, as compared to Groups A and C. However, the concentration of large oxide inclusions ($\sqrt{\text{Area}} > 10$ or $> 20 \mu\text{m}$) was significantly higher in Group B, and was not proportional to oxygen content. For example, the concentration of oxides greater than $10 \mu\text{m}$ was about nine times higher in Group B, compared to Group C (Table 2A). This lack of proportionality was also illustrated by the DIN 50602 K0 – K4 cleanliness (OA + OG) results (Fig. 2A). Furthermore, although Groups A and C had the same oxygen content (7 ppm), Group A had a higher concentration of large oxide inclusions and higher DIN 50602 K0–K4 cleanliness (OA + OG) results. These results indicate that the concentration of large oxides does not necessarily depend on the oxygen content. Therefore, the oxygen content does not fully predict the nature of the oxide inclusion population.

In regard to sulfide inclusions, the total sulfide area, as well as the area of large sulfide inclusions, was linearly related to the sulfur content of the steel. Group C had a sulfur content that was three times higher than Groups A and B, and

| Sample Group | C | Mn | P | S | Si | Cr | Ni | Mo | Cu | Al | Ca* | O* _{Tot} | N* |
|-----------------------------|------|------|-------|-------|------|------|------|------|------|-------|-----|-------------------|-----|
| A Low O Low S | 0.41 | 0.97 | 0.013 | 0.007 | 0.29 | 0.90 | 0.14 | 0.15 | 0.22 | 0.024 | 3 | 7 | 97 |
| B High O Low S | 0.41 | 0.96 | 0.014 | 0.008 | 0.29 | 0.90 | 0.14 | 0.15 | 0.22 | 0.022 | 4 | 15 | 97 |
| C Low O High S | 0.41 | 0.94 | 0.014 | 0.024 | 0.19 | 0.88 | 0.11 | 0.18 | 0.22 | 0.027 | 1 | 7 | 119 |

*Calcium, total oxygen, and nitrogen concentrations given in ppm.

| Sample Group | Oxygen Content (ppm) | Total Oxide Area | Conc. $\sqrt{A} > 10 \mu\text{m}$ $\sqrt{A} > 20 \mu\text{m}$ | Oxide Stringer Length $L > 100 \mu\text{m}$ $L > 200 \mu\text{m}$ | SEV Oxide $\sqrt{\text{Area}} (\mu\text{m})$ Stringer Length (μm) | UT Metric (Oxides) | DIN 50602 (Oxide) OG+OA K1/K4 |
|--------------|----------------------|------------------|---|---|--|--------------------|-------------------------------------|
| A | 7 | 29.07 | 2.17 0.07 | 1.19 0.36 | 26.06 285 | 0.469 | 0.82/0.29 |
| B | 15 | 56.98 | 7.45 0.46 | 20.82 8.36 | 52.79 801 | 1.798 | 3.92/1.21 |
| C | 7 | 20.14 | 0.81 0.07 | 2.10 0.46 | 20.41 416 | 0.678 | 0.28/0.0 |

| Sample Group | Sulfur Content (wt. %) | Sulfide Area Total $L > 100 \mu\text{m}$ | DIN 50602 (Sulfide) SS K1/K4 |
|--------------|------------------------|---|------------------------------------|
| A | 0.007 | 208.2 45.6 | 5.09/0.0 |
| B | 0.008 | 199.4 50.2 | 5.51/0.0 |
| C | 0.024 | 565.1 111.5 | 13.56/0.0 |

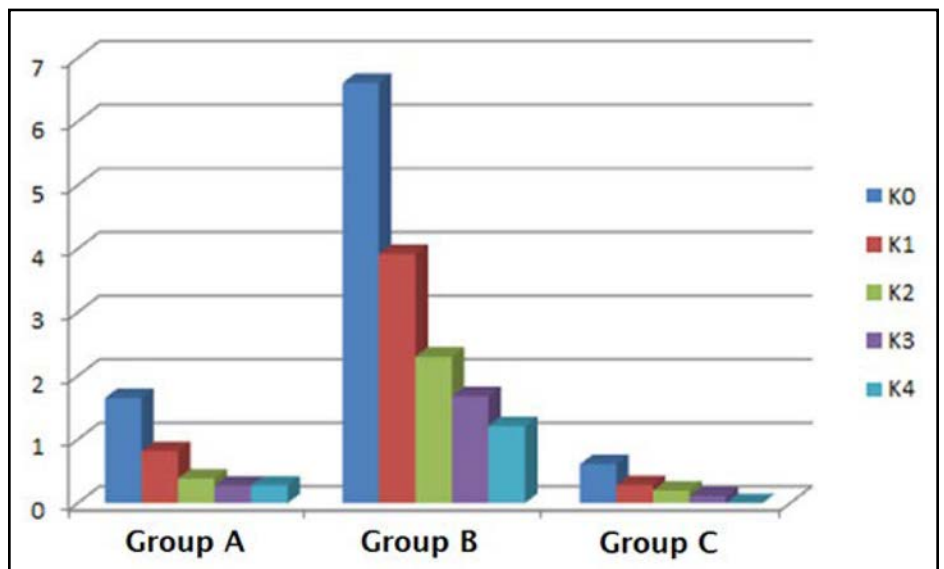


Figure 2A DIN 50602 K0—K4 cleanliness (OA+OG) results for the three sample groups.

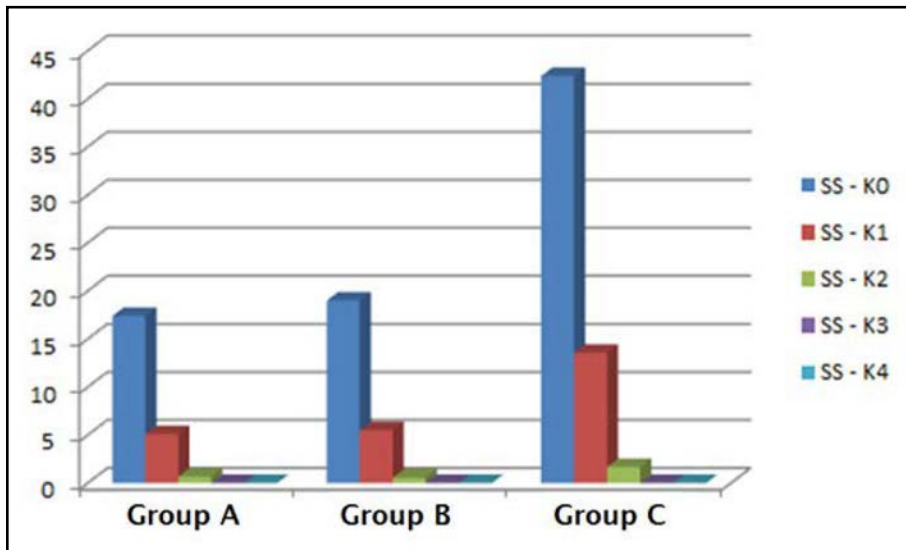


Figure 2B DIN 50602 K0—K4 sulfide cleanliness (SS) results for the three sample groups.

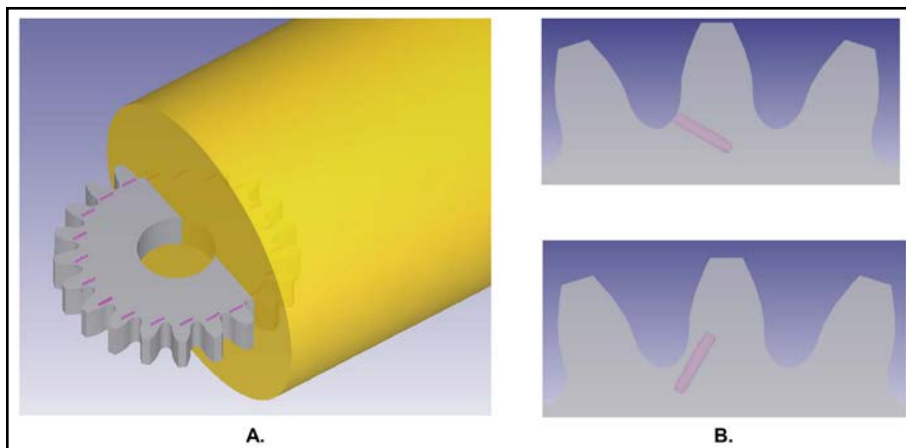


Figure 3 Orientation of spur gears machined from as-rolled bar stock (A), and the inclusion orientations (B), in the longitudinal test position (lower photo) and transverse position upper photo).

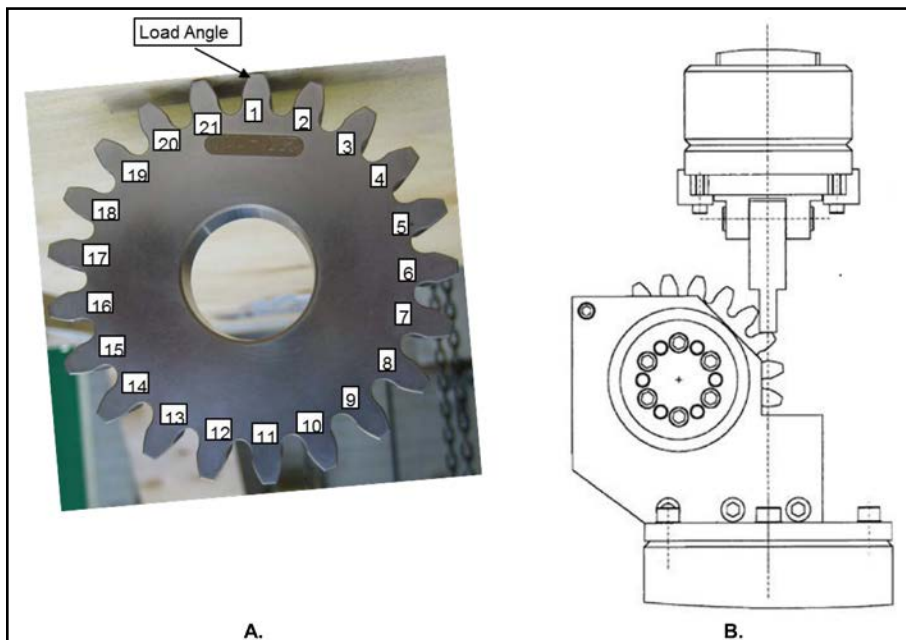


Figure 4 Machined spur gear with numbered teeth for testing showing the loading angle (A), and the testing fixture showing the loading gear tooth in the cyclic R=0.1 loading condition (B).

all sulfide inclusion metrics were also approximately three times higher (Table 2B and Fig. 2B). It is important to note that the sulfide count and area metrics were significantly greater than the oxide count and area metrics in all sample groups. Even the high-oxygen/low-sulfur samples (Group B) showed that the concentration of the large sulfides ($>100 \mu\text{m}^2$) was more than four times greater than the concentration of the large oxides ($>100 \mu\text{m}^2$).

Fatigue Testing

Single tooth-bending fatigue. 4.2 modulus spur gears were manufactured from each steel condition (A, B, and C) and oriented such that both longitudinal and transverse orientations — with respect to inclusion orientation — were bending fatigue tested at the gear teeth root locations (Fig. 3). The gear steel blanks were through-hardened as follows: austenitized at 885°C (1,625°F) for 30 minutes at temperature, oil-quenched and tempered at 177°C (350°F) for one hour to an average hardness of 55 HRC (~595 Hv). Following heat treat, the gears were finish machined, followed by controlled, dual shot peening to maximize the near-surface compressive stress state in the tooth root area.

The 4140 spur gears were tested on a single tooth bending testing rig (Fig. 4) at one of five pre-selected loads with a load ratio of $R=0.1$, until root bending fatigue failure occurred, or a run-out condition was met (10^7 cycles). Tests were repeated three times at each load for all steel conditions and orientations, and an average value for each test sequence was calculated to compare to one another. The generation of an endurance limit — or fatigue strength — based on various runout conditions was not a goal of this testing mode, as compared to the other two test types, and will not be compared to those tests in that method. The fractured gear teeth were examined under an FE-SEM to locate the initiation site(s), and in the case of inclusion origin failures, the type of the inclusion was documented.

Brugger bending fatigue. Modified Brugger bending fatigue specimens (Fig. 5) are designed to simulate a gear tooth root bending condition. The failures occur nearly perpendicular to the

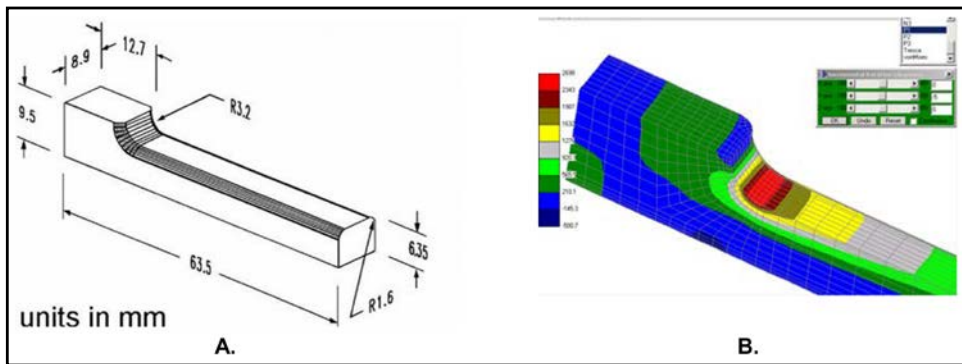


Figure 5 Bruggen specimen print dimensions (A), and the maximum loading stress profile imposed by the cyclic $R=0.1$ loading condition (B).

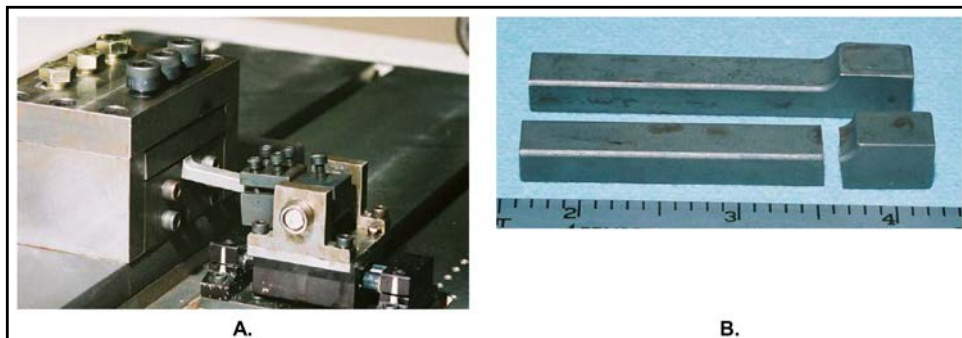


Figure 6 Bruggen test machine setup (A) and as-manufactured-and-tested to failure specimens (B).

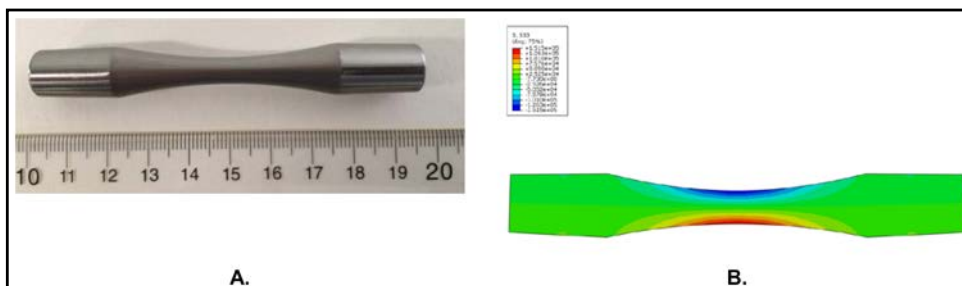


Figure 7 Image of the RBF test (RR Moore) specimen (scale shown in mm) (A), and a typical stress profile during loading (B).

length of the specimen (Fig. 6B) and, as such, longitudinal and transverse blanks were cut from as-rolled bar along the length and transverse to the length to represent these orientations. The Bruggen specimens were machined from the blanks to a 16 micro-inch surface finish prior to heat treatment. The specimens were austenitized at 885°C (1625°F) for 30 minutes at temperature, oil-quenched and tempered at 177°C (350°F) for one hour to an average hardness of 55 HRC (~595 Hv). The finished specimens were then controlled dual shot peened to provide a near-surface compressive stress layer.

Testing was performed at various loads to a ratio of $R=0.1$ until failure or a runout condition was met (10^7 cycles). Testing was performed until a

complete S-N type fatigue curve was developed — including multiple runout failures at loads where no failures occurred — to determine an endurance limit for each steel condition and orientation. The fractured specimens were examined under an FE-SEM to locate the initiation site(s) and, in the case of inclusion origin failures, the type of the inclusion was documented.

Rotating bending fatigue (RBF). Longitudinal (i.e., parallel to the rolling direction) and transverse (i.e., perpendicular to the rolling direction) RBF specimens from the three sample groups (A, B, and C) were manufactured from the mid-radius portion of the representative bars. The test samples were austenitized at 885°C (1,625°F) for 30 minutes at temperature, oil-quenched and tempered at

177°C (350°F) for one hour to an average hardness of 55 HRC (~595 Hv). Following the heat treatment, the specimens were finish machined, ground, and polished along the specimen axis to an axial $Ra < 2.5 \mu\text{in}$ (0.06 μm) and a circumferential $Ra < 2.0 \mu\text{in}$ (0.05 μm). An image of the RBF test (RR Moore) specimen and a typical stress profile are shown (Fig. 7).

The 4140 samples from the A, B and C sample groups were fatigue tested in the fully reversing/rotating bending test rig (i.e., stress ratio; $R=-1$ and mean stress; $\sigma_m=0$). A minimum of 12 (in most cases, 16 or more) test specimens from each of the three groups ($\times 2$ orientations) were run to generate comparative S-N curves. At least two specimens from each group were run at each loading condition. The selected suspension criteria (i.e., runout

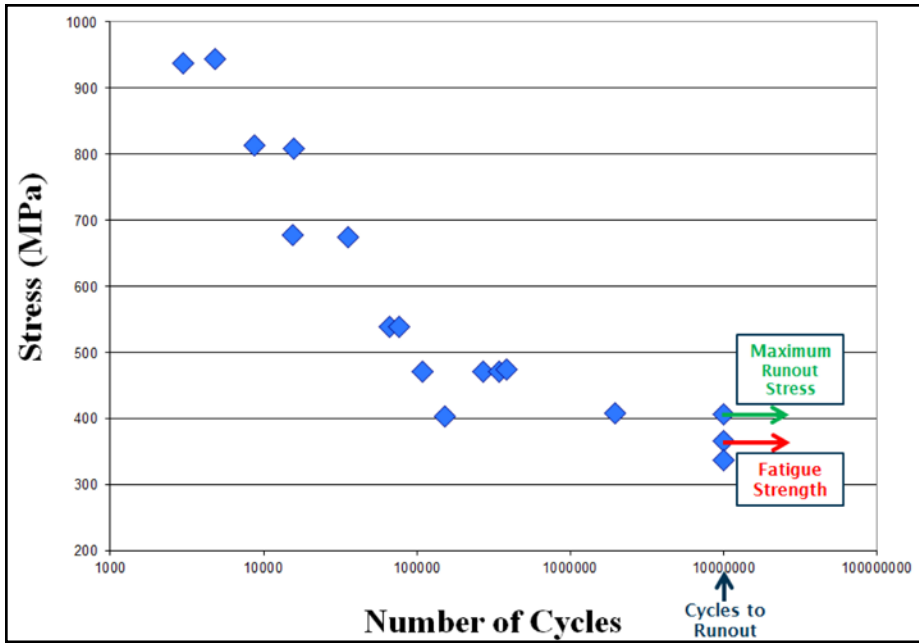


Figure 8 A depiction of how the key metrics were determined from the S-N type curve data.

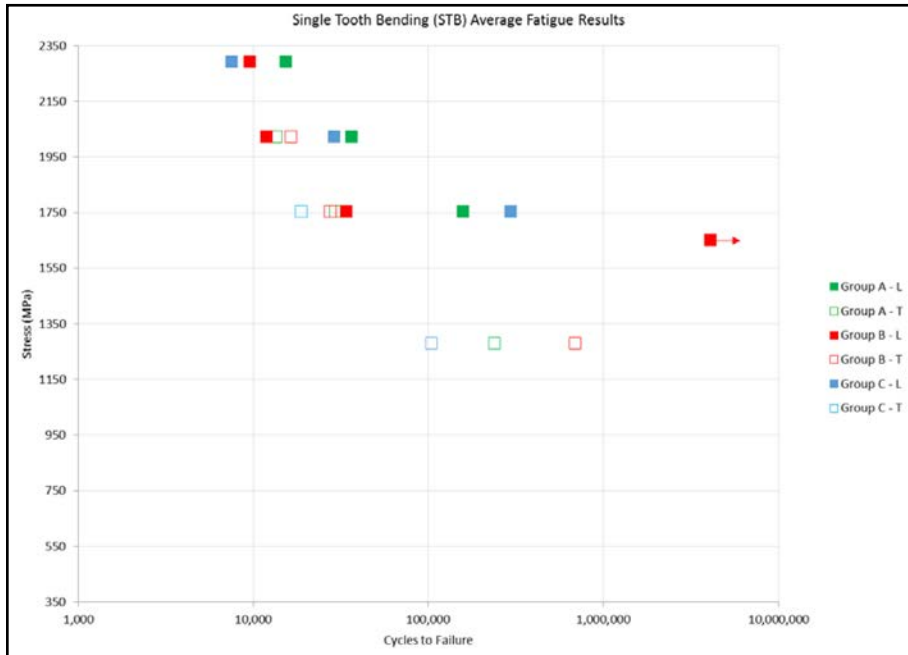


Figure 9A

bogey) was 10^7 cycles.

The fracture surface of failed test specimens was evaluated using an FE-SEM to determine the initiation point of the fatigue failure. If the fatigue crack initiated at an inclusion, the type was noted.

Two key fatigue metrics were measured for the Brugger and RBF tests. The maximum runout stress (MRS), as the name implies, was the highest stress level at which at least one specimen in a given test group reached the test suspension bogey. The second metric was fatigue strength (FS) (note that the fatigue strength is occasionally referred to as fatigue or endurance limit.), defined as the maximum stress level, at or below which no samples within a group failed. These two metrics are graphically displayed in one of the experimentally generated S-N curves (Group C – Transverse Orientation) shown in Figure 8.

Results

Fatigue results. The fatigue results generated from these three bending fatigue testing methods on the three steel cleanliness conditions and two orientations are presented in Figures 9 A, B, and C. The fatigue strength and maximum runout stress for the Brugger and RBF tests for each sample group and orientation are listed in Table 3. These results essentially compare the testing methods, the steel conditions, and the orientation effects that were tested within this overall effort.

Test type comparison. Based on the test results in Figure 9 and Table 3, it is apparent that fatigue performance was highly dependent on the test type. STB testing consistently had the highest cycles to failure at a given stress level, followed by Brugger testing (~20% lower than STB), and RBF testing (30% to 50% lower than Brugger testing). Similarly, the Brugger test showed higher fatigue strengths and maximum runout stresses than the RBF test (Table 3). Only one runout was obtained for STB testing, for a longitudinal Group B sample tested at 1,650 MPa — well above the maximum runout results for either of the other test methods.

Both the STB and Bruggen tests had a cyclic loading ratio (R value) of 0.1, while the RBF test had a cyclic loading ratio of -1. The test results were contrary to the expectation that the RBF test (R=-1) would produce the highest fatigue strength due to the lowest average stress (0). Both the STB and Bruggen tests (R=0.1) had a positive average stress. A possible explanation for the unexpected relationship between test type and fatigue performance will be explored in the discussion section of this paper.

Steel variant and orientation comparison. The fatigue test results showed that sample orientation had a significant effect on fatigue performance. In RBF testing the fatigue strength of the transverse samples was about one-half of the longitudinal samples, and in Bruggen testing it was about one-half to two-thirds. A fatigue strength was not determined in STB testing; however, the transverse samples had fewer cycles-to-failure at a given stress level than the longitudinal samples.

In testing of longitudinal samples, Group B (high oxygen) generally had the lowest fatigue performance. Specifically, in longitudinal STB testing, Group B had significantly fewer cycles-to-failure at the stress levels of 1,753 MPa and 2,022 MPa. At 1,753 MPa, Group B had 78% and 88% fewer cycles than Groups A and C, and at 2,022 MPa, Group B had 67% and 59% fewer cycles, respectively. In longitudinal Bruggen tests, the fatigue strength and maximum runout only varied by about 4% between the sample groups. This suggests that the inclusion population had a limited effect on the longitudinal Bruggen test. However, in longitudinal RBF tests the high-oxygen steel (Group B) had 8–16% lower fatigue strength and maximum runout stress than the two low-oxygen steels. Due to the differences in performance between the low-oxygen steels, the fatigue results were also compared with respect to the concentration of large oxide inclusions. This analysis revealed that the fatigue performance showed a better correlation to the concentration of large oxide inclusions than to oxygen content (Fig. 10A).

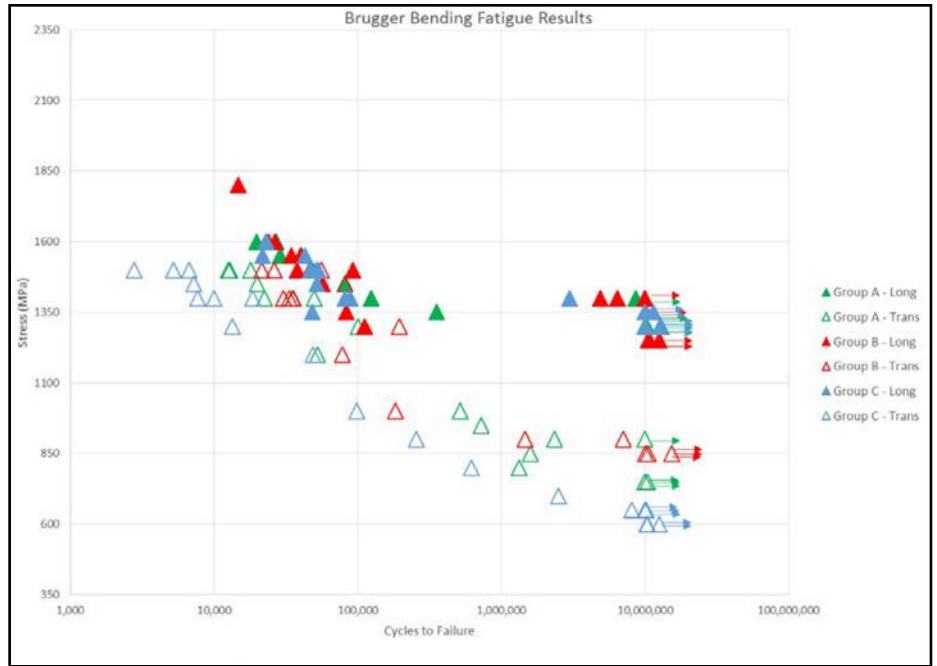


Figure 9B

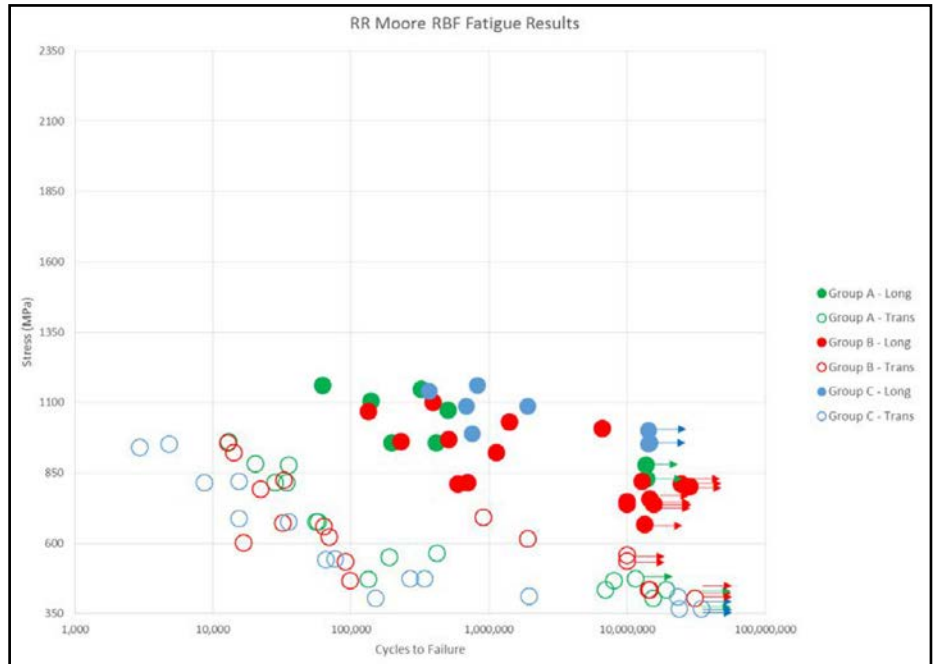


Figure 9C

Figure 9 Fatigue plots for the A—STB (each point is an average of 3 tests; B—Bruggen and C—RBF plots for all steel groups.

Table 3 Fatigue strength values (FS) and maximum runout stress (MRS) for the Bruggen and RR Moore RBF tests for each steel condition and orientation.

| Sample Orientation | Longitudinal | | | Transverse | | |
|---|--------------|---------|---------|------------|---------|---------|
| | Group A | Group B | Group C | Group A | Group B | Group C |
| Oxygen Content (ppm) | 7 | 15 | 7 | 7 | 15 | 7 |
| Oxide Conc. $\sqrt{A} > 10 \mu\text{m}$ | 2.17 | 7.45 | 0.81 | 2.17 | 7.45 | 0.81 |
| Sulfur Content (wt%) | 0.007 | 0.008 | 0.024 | 0.007 | 0.008 | 0.024 |
| Bruggen FS (MPa) | 1300 | 1250 | 1300 | 750 | 850 | 600 |
| Bruggen MRS (MPa) | 1400 | 1400 | 1350 | 900 | 850 | 650 |
| RBF FS (MPa) | 877 | 804 | 955 | 412 | 402 | 366 |
| RBF MRS (MPa) | 967 | 882 | 999 | 527 | 533 | 407 |

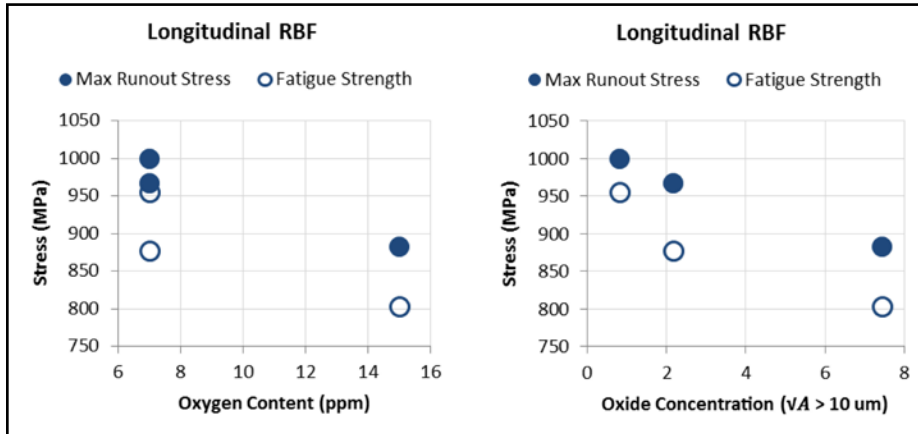


Figure 10A Plots showing RBF fatigue performance vs. oxygen content (left); and the concentration of large oxides (right).

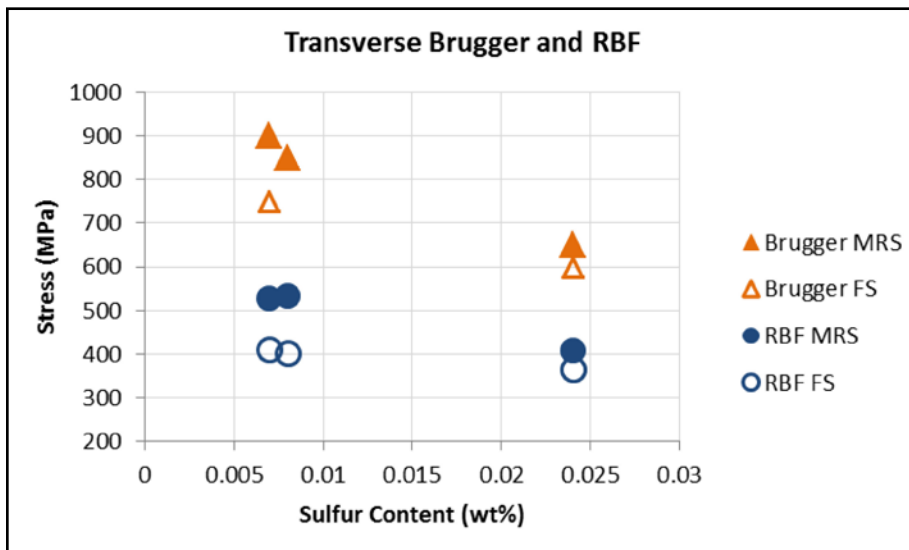


Figure 10B Plot showing transverse Brugger and RBF fatigue performance vs. sulfur content.

In testing of transverse samples, Group C (high sulfur) consistently had the lowest fatigue performance. In transverse STB testing, Group C had 57% and 85% fewer cycles at 1,281 MPa than Groups A and B, and 36% and 32% fewer cycles at 1,753 MPa, respectively. In transverse Brugger testing the fatigue strength of Group C was about 20–30% lower than groups A and B. In transverse RBF testing, Group C had a fatigue strength that was about 10% lower than both Groups A and B. The effect of sulfur content on fatigue strength and maximum runout stress in Brugger and RBF testing is illustrated in Figure 10B.

Fractography results. The fracture surface of a majority of the failed test specimens were examined by scanning electron microscopy (SEM) in order to locate and characterize the fracture initiation site(s). All fracture initiation sites were located either at a non-metallic inclusion or at the specimen surface with no inclusion present. In cases where fracture initiation occurred at a non-metallic inclusion, the initiation sites were further categorized by inclusion type (oxide, sulfide, etc.). The number of fracture initiation sites (single vs. multiple) was also noted. Examples of a surface, oxide, and sulfide initiation site are shown (Fig. 11).

Specimen orientation and sample group comparison. In Figure 12 the frequency of each fracture initiation type by sample group and orientation is shown for each test method. As illustrated in the figure, specimen orientation had a dramatic effect on fracture initiation type. Transverse specimen fractures were predominantly sulfide-initiated while longitudinal specimen fractures were largely surface-initiated or oxide

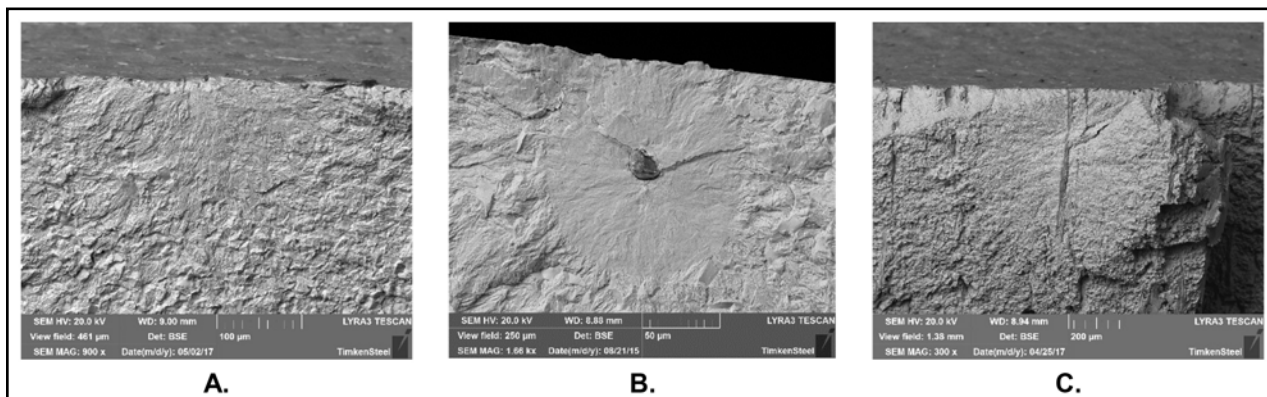


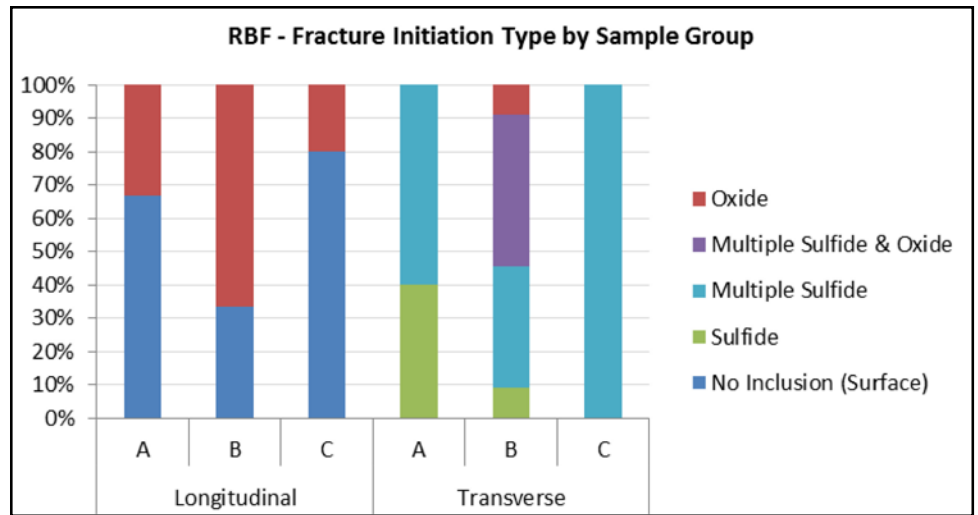
Figure 11 SEM images showing a surface initiation site with no inclusion (A); an oxide initiation site (B); and a sulfide initiation site (C).

inclusion-initiated. When data from all test methods and sample groups were combined, 88% of all transverse specimen fractures were sulfide-initiated, compared to just 1% of longitudinal specimens.

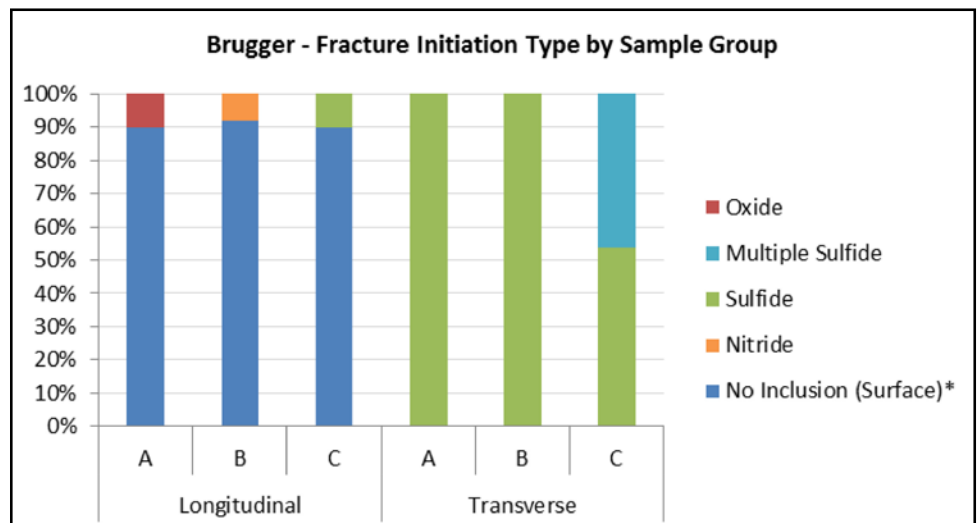
In Brugger and STB testing of longitudinal specimens, nearly all fractures were surface-initiated and little group-to-group variation was observed. It is worth noting that 52% of surface initiations in Brugger testing were located at the corner (surface transition from horizontal to the R1.6 radius) of the specimen. In RBF testing of longitudinal specimens a significantly higher rate of oxide inclusion initiation was observed in Group B (high concentration of large oxides) compared to Groups A and C. Oxide inclusions initiated 67% of longitudinal Group B failures, compared to 33% and 20% in Groups A and C, respectively.

In testing of transverse specimens, Group C (high sulfur) had the highest frequency of multiple sulfide initiation sites for all test methods. In RBF testing, 100% of transverse Group C specimens had multiple sulfide initiation sites, and in Brugger and STB testing, the frequency was approximately 50%.

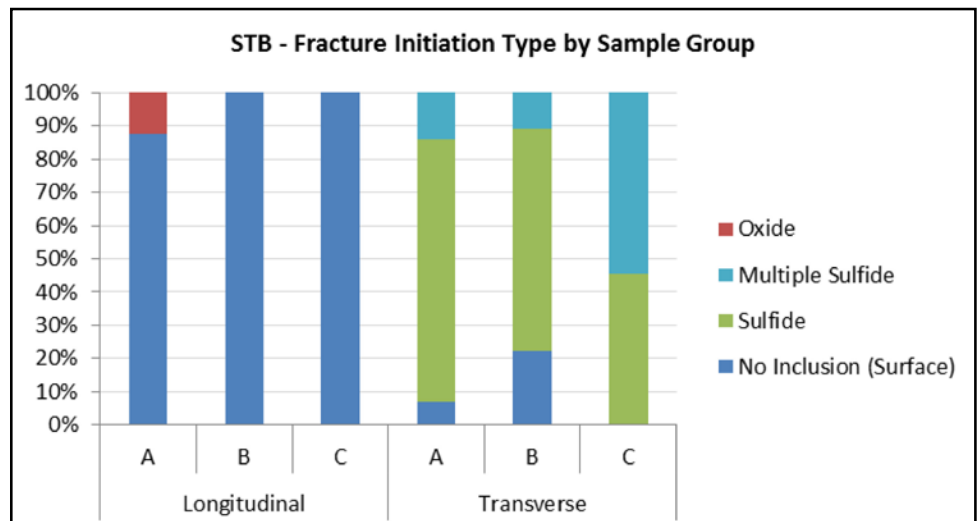
Magnitude of applied Stress. In addition to sample orientation and sample group, the level of applied stress also had a significant effect on the fracture initiation type of longitudinal specimens. At stress levels where multiple failures were observed, inclusion-initiated failures increased in frequency with decreasing applied stress (Fig. 13). In RBF testing, the frequency of inclusion initiations was 80% at 900 to 1,000 MPa, 50% at 1,000 to 1,100 MPa, and 25% at 1,100 to 1,200 MPa. Similarly, in Brugger and STB testing, inclusion-initiated failures were only observed at the lowest level of applied stress at which multiple failures occurred.



A

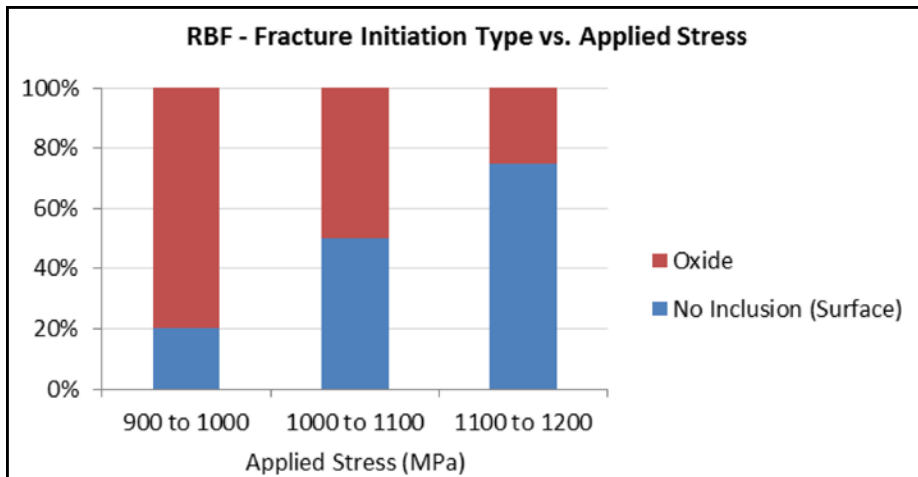


B

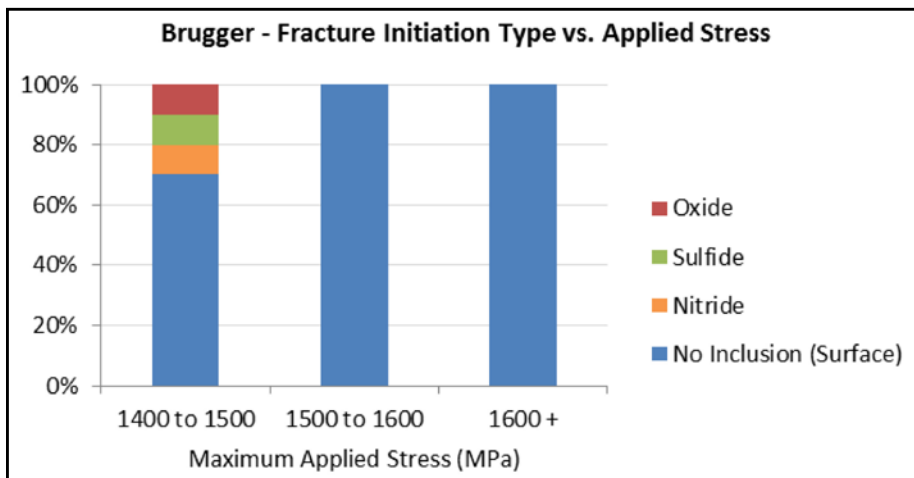


C

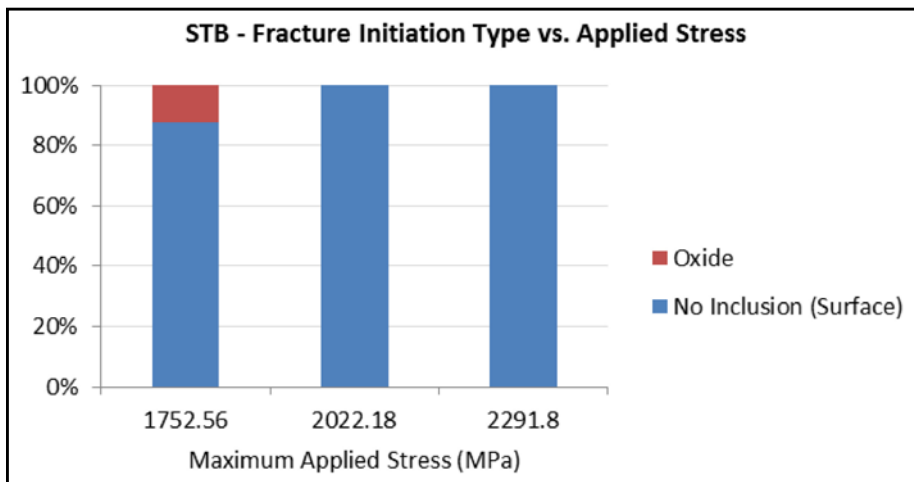
Figure 12 Plots showing the frequency of each fracture initiation type (oxide, sulfide, etc.) by sample group and orientation in RBF testing (A); Brugger testing (B); and STB testing (C).



A



B



C

Figure 13 Plots showing the frequency of each fracture initiation type (oxide, sulfide, etc.) of longitudinal specimens vs. the maximum applied stress in RBF testing (A); Bruggen testing (B); and STB testing (C).

Discussion

As noted previously, the RR Moore RBF results present some of the more interesting results in regard to the effects of inclusions on fatigue properties. As such, the primary test for discussion will be the RBF results and the impact of the inclusion population on the fatigue properties for this test mode. However, the discussion will begin by comparing the three different test types and the types of information obtained from each. It was noted that there was a large discrepancy in fatigue results between these tests, i.e. — on the order of nearly a factor of 2 between the highest and lowest test results for the same steel conditions.

Single-tooth bend test. The higher-stress/cycle results observed in the single-tooth bend test — as compared to the other tests for all steels and orientations — suggests a difference in this test method compared to the other methods. It is also apparent that the peened surface on these samples was not effective in preventing surface initiation and may have resulted in an overriding degradation of surface finish, which resulted in the high quantity of surface failures. Since most of the longitudinal tests were surface-initiated, while most transverse tests were inclusion-initiated, it is unlikely that the effect was due to a surface stress condition.

However, this test did in fact differentiate between the low and high oxide levels in the longitudinal orientation, showing lower cycles to failure for the higher-oxide group (showed similar results to transverse tests), indicating that the dirty steel condition resulted in a significant compromising of the STB fatigue results. This was true even though the initiation location of many of the longitudinal tests was at the surface rather than at a subsurface inclusion. The transverse test showed the general reduction in fatigue properties, as compared to longitudinal, and the cycles to failure tended to trend opposite the volume of inclusions present, with multiple initiation sites resulting in the lowest cycles to failure.

Bruggen bending test. The Bruggen stress/cycle results were intermediate, as compared to the other two tests, possibly for reasons, described later on, related to stressed volume factors. This test also suffered from a high quantity of surface

failures in the longitudinal orientation, indicating that the compressive stresses on the peened surface may not have been effective at preventing surface-initiated failures. Furthermore, a large number of the surface initiation sites (52%) were located at the corner of the Brugger specimen, suggesting that a geometric stress concentration promoted fracture initiation at this location. As a result inclusions played a very limited role in failure of the longitudinal specimens, and the high-oxide variant had only 4% lower fatigue strength. The sulfides dominated the transverse fatigue origin sites for each steel variant and applied load, resulting in a relationship between sulfur level and fatigue strength. As such, this test was probably least sensitive to inclusion content, type, and orientation, requiring more macro shifts between the steel variants to affect the fatigue performance.

RR Moore rotating bending test. A number of observations can be extracted from the measured RBF fatigue data. Perhaps the most apparent information from the S-N data (Figs. 9 and 10; Table 3) is that the transverse samples from each sample group displayed significantly lower fatigue life at a given load, and about half the fatigue strength than found for the corresponding longitudinal samples. Experimental data from an early study by Sumita et al. (Ref. 5) revealed a corresponding difference in fatigue strength between longitudinal and transverse specimens in medium- and high-strength steels ($H_v > 300$), but no cause was assigned. The measured fatigue strength ratios from the current study are in reasonable accord with reported ratio values found in the literature (Ref. 6). Upon closer inspection of the data, the ratio of longitudinal- to transverse-measured fatigue strengths appears to be a function of sulfur content of the steel (Fig. 14). This may be expected, given that the measured total inclusion areas (oxides + sulfides, but dominated by sulfides) perpendicular to the applied stress for Group C were more than twice that of either Group A or B.

Further review of the fatigue data with regard to inclusion population metrics on the transverse specimen indicates that the high-sulfur sample group (C) displayed the poorest fatigue performance in this orientation. The measured fatigue

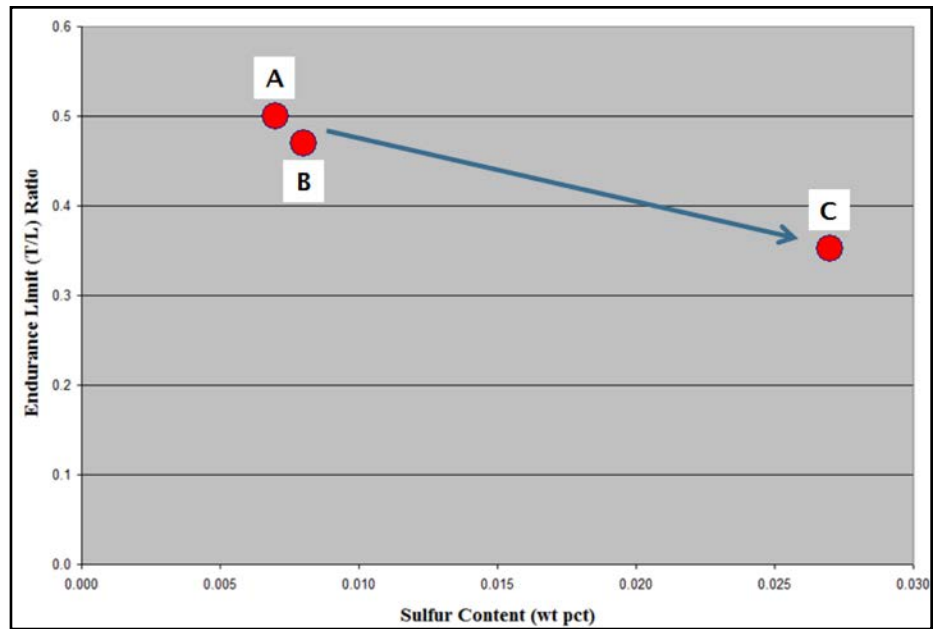


Figure 14 Ratio of transverse to longitudinal fatigue strengths plotted as a function of sulfur content.

strength of the C samples, containing 0.024% S, was about 10% below that measured on sample groups A and B, which contained about one-third the sulfur and, equivalently, had approximately one-third the measured sulfide area.

The S-N results on the longitudinal samples were more scattered than was found with the transverse samples. This may be due to the initiation location (both radially and axially) differences between these two orientations, as discussed later. Still, it is clear that the high-oxide sample group (B) had approximately a 10 to 15% lower MRS and FS than the two low-oxide sample groups. This result is in directional accord with findings reported in the literature (Refs. 7–9).

These effects in both sample orientations are clearly shown (Figs. 15A and 15B). The fatigue metric (MRS and FS) values for the longitudinal samples are plotted as a function of the oxide cleanliness in terms of DIN 50602 (OG+OA) K1 values (Fig. 15A), while the fatigue metric values for the transverse samples are plotted as a function of the sulfide population, as defined by the measured DIN 50602 SS K1 values (Fig. 15B).

Another observation from this study was the reasonably consistent difference in the location of the fatigue fracture along the specimen axis between longitudinal and transverse test specimens.

Given the hour-glass geometry of the standard RBF test (RR Moore) specimen, the highest tensile stresses in the

absence of internal defects (e.g., non-metallic inclusions) and surface imperfections occur at the surface of the mid-point of the sample. Accordingly, it may be expected that most of the test samples would fracture at or very near the mid-length of the specimen. As shown in Figure 16, the measured length difference of the mating halves of the failed test specimen indicated that average axial fracture location on the transverse samples was significantly and consistently closer to the mid-length point of the specimen than was found with the longitudinal samples.

This observation may be reflective of the following facts: the fatigue failures in the transverse samples were primarily associated with MnS stringers, which were significantly more abundant (and likely more uniformly distributed) than the oxide inclusions where most of the failures in the longitudinal samples occurred. Accordingly, there would be a greater probability that the highest stresses would occur closer to the mid-length position in the transverse samples. Whereas in the longitudinal inclusion-initiated samples the highest stresses would be a combination of the applied and local stresses located around the inclusion. This may also account for the higher level of scatter in the longitudinal data, as this combination of stresses would be dependent both on the applied load and the inclusion population present.

The results of the current study

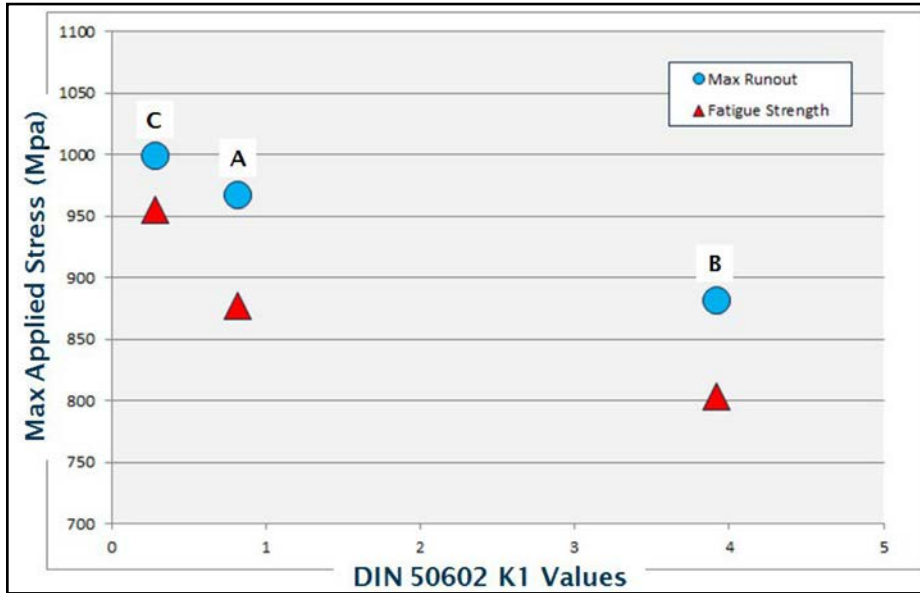


Figure 15A Fatigue metrics of longitudinal samples plotted as a function of oxide cleanliness.

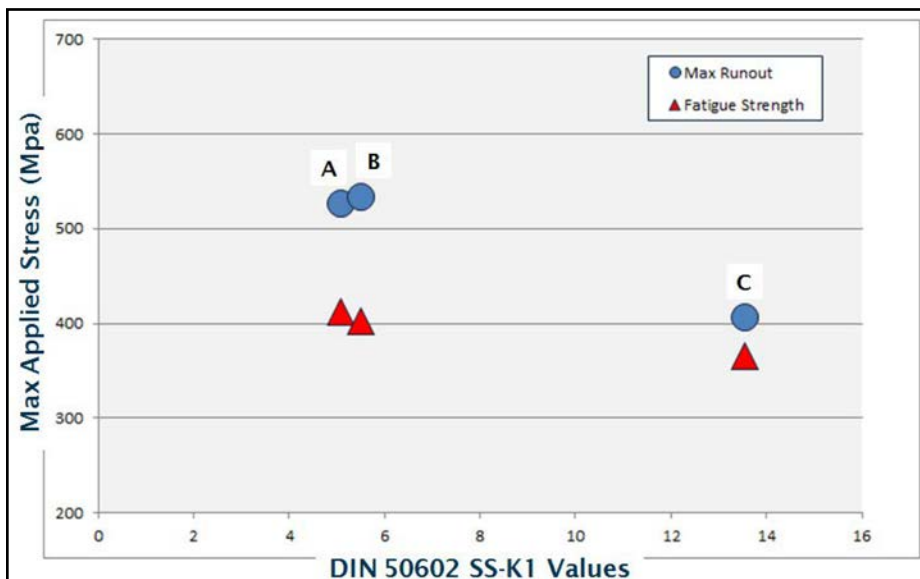


Figure 15B Fatigue metrics of transverse samples plotted as a function of sulfide cleanliness.



Figure 16 Images of typical transverse and longitudinal failed test specimens, illustrating the difference in axial failure location. The average axial distance of the fracture surface from the specimen mid-length (and corresponding standard deviation) are provided.

demonstrate the adverse effect of oxide inclusions on the fatigue life in the axial orientation. While a 10 to 15% difference in fatigue strength between the high- and low-oxide sample sets is not particularly large, the difference has been shown to be statistically significant. Furthermore, this detrimental effect of oxide population is directionally consistent with results reported in much of the literature (Refs. 7–13).

One possible explanation for the smaller-than-expected effect on fatigue performance is related to stressed volume. As recently reported, axial fatigue studies by Furuya (Ref. 14) on SCM440 steel (similar to 4140) demonstrated the importance of relative stressed volume when evaluating the impact of steel cleanliness (oxide population) on fatigue performance of two specimen sizes. The detrimental impact of cleanliness on fatigue was observed with both specimen types. However, the single melt (higher oxygen) larger specimen that had a calculated stressed volume of 781 mm³, showed 25% lower fatigue strength than the double-melt (low-oxygen) samples. While in the smaller specimen, with a stressed volume of only 33 mm³, the difference was between 5 and 10%.

Interestingly, in the current study both the measured 10 to 15% difference in fatigue strength between the high- and low-oxygen sample groups and calculated stressed volume of the RBF specimen, about 23 mm³, were both very similar to the results with the smaller specimen used in Furuya's work.

The size of the stressed volume may also offer a possible reason for the discrepancy in fatigue performance between

the three tests. The RBF specimen had the highest stressed volume (about 23 mm³) and the lowest fatigue performance. The Brugger specimen had an intermediate stressed volume (about 5 mm³) and an intermediate fatigue performance relative to the two other tests. Finally, the STB specimens had the smallest stressed volume (about 4 mm³) and the highest fatigue performance.

Summary

Three sample sets of quenched and tempered 4140 steel, with varying levels of oxygen and sulfur, were submitted to a series of single-tooth bending, Brugger bending, and rotating bending fatigue tests. Test specimens were prepared in both longitudinal and transverse orientations.

Oxide and sulfide inclusion populations of all three sample sets were thoroughly characterized employing both SEM image analysis and high-resolution ultrasonic methods. The key cleanness metrics were in reasonable accord with the measured total oxygen and sulfur contents of the steel sample sets.

The following observations and conclusions can be drawn from this study:

The oxygen contents of the steels did not fully predict the nature of the oxide inclusion populations. Based on SEM-based image analysis, Group B had roughly twice the oxygen content of Group C, but the concentration of large oxides ($\sqrt{\text{Area}} > 10 \mu\text{m}$) was about nine times greater. Furthermore, Groups A and C had the same oxygen content, yet the concentration of large oxides in Group A was three times greater than in Group C.

Sample orientation had a significant effect on the fatigue performance and failure modes in each of three test methods. In RBF testing the fatigue strength of the transverse samples was about one-half of the longitudinal samples; in the Brugger testing it was about one-half-to-two-thirds. In STB testing a fatigue strength was not determined; however, the transverse samples had fewer cycles to failure at a given stress level than the longitudinal samples. In each test method a large majority of transverse failures were sulfide inclusion-initiated, while very few longitudinal failures were sulfide-initiated.

The fatigue performance and failure

mode of transverse samples was dependent on the sulfur content of the steel. The high-sulfur sample set (Group C) had approximately 10% lower fatigue strength in RBF testing, and approximately 20–30% lower in Brugger testing. In STB testing, Group C samples had consistently fewer cycles to failure. In all test methods, Group C had a high frequency of failures with multiple sulfide initiation sites (as opposed to a single initiation site).

The fatigue performance of longitudinal samples in RBF and STB testing was dependent on the concentration of large oxide inclusions. Furthermore, the concentration of large oxide inclusions provided a better prediction of fatigue performance than oxygen content. In RBF testing, Group B (highest concentration of large oxides) had a fatigue strength that was 8% lower than Group A and 16% lower than Group C. In STB testing, Group B samples had 59 to 88% fewer cycles to failure at a given stress level. In RBF testing, the failure mode of longitudinal samples was also dependent on the concentration of large oxides. Group B had the highest rate of oxide-initiated failures (67%), followed by Group A (33%) and Group C (20%).

References

1. Murakami, Y. "Metal Fatigue: Effects of Small Defects and Nonmetallic Inclusions," Elsevier, London, Ch. 6, 2000.
2. Erickson, M.A., M.F Garwood and H.H. Zurburg. "Interpretation of Tests and Correlation with Service, American Society of Metals," 1951.
3. Nishijima, S. "Statistical Analysis of Fatigue Test Data," *Journal of the Society of Material Science, Japan*, Vol 29, 1980, pp. 24–29.
4. Homma, H. and H. Nakazawa. "Fatigue Strength of Metals," Yokendo Ltd., Tokyo, pp. 25; 1992.
5. Araki, T., M. Sumita and I. Uchiyama. "The Effect of Inclusions on Fatigue Properties of Steel with Various Matrixes," *Tetsu to Hagane*, 57(2), pp. 298–334, 1971.
6. Boardman, B. *ASM Handbook: Properties and Selection: Irons, Steels and High-Performance Alloys*, ASM International, Vol. 1, p. 683, 1990.
7. Firth, P.H. "Fatigue Tests on Rolled Steel Made in Electric and Open-air Furnaces," *Journal of the Iron and Steel Institute*, Vol. 80, pp. 26–33, 1955.
8. Forrest, P.G. *Fatigue of Metals*, Pergamon Press, pp. 64–65, 1962.
9. Adachi, A., Y. Inoue, A. Kuwabara and H. Shoji. "Rotating Bending Fatigue Phenomenon of JIS SUJ2 Bearing Steel," *Elect. Furnace Steel*, Vol. 46, pp. 176–182, 1975.
10. Machida, H. *Technology of a Traction Drive CVT – Past, Present and Future*, D. Dowson, et al. (Eds), Elsevier B. V., 2005.
11. Rösch, S. and W. Trojahn. "Steel Cleanliness and Bearing Life," *Bearing Steel: Advances in Rolling*

Contact Fatigue Strength Testing and Related Substitute Technologies: STP 1548, ASTM, pp. 102–113, 2012.

12. Gabelli, A., et al. "Rolling Bearing Material Quality Fatigue Testing — Material Quality Life Factors," *Bearing Steel Technology: STP 1419, ASTM*.
13. Adkinson, C.W., H.V Anderson, C.M. Sellars, G. Shi and J.R. Yates. "Fatigue Tolerant Design of Steel Components Based on the Size of Large Inclusions," *Fatigue Fracture Engineering of Material Structures*, Vol. 25, pp. 667–677, 2002.
14. Furuya, Y. "Gigacycle Fatigue Properties of Double Melted SCM440 and Size Effects," *ISIJ International*, 54(6), pp. 1436–1442, 2014.

For Related Articles Search

gear steel

at www.gearstechnology.com

Michael Burnett, a

technologist at the Timken Steel corporation, earned a Bachelor's degree from Purdue University and a Master's degree from the Colorado School of Mines—both in Metallurgical Engineering before joining the company 35 years ago. He has since worked primarily in a technical capacity developing and implementing advanced engineered steels and technologies for crankshafts, gears, bearings and other demanding applications, with an emphasis on improving both the manufacturing and performance characteristics.



Peter Glaws is a senior

scientist-materials (since 2014) at Timken Corp, and has worked at Timken received his (BS) metallurgical engineering degree at Lafayette College in 1977. After four years (1977–1981) working in the steel industry, he returned to academia (1981–1985), moving on to Carnegie Mellon University where (1981–1985) he received his PhD in materials engineering. After two years (1985–1987) as a doctoral fellow at the University of Newcastle, NSW Australia, Glaws joined Timken Corp. (1987), where he has held various senior technical positions, including his present senior scientist position.



Daniel Gynther is a senior metallurgical

development engineer at TimkenSteel Corporation. Since joining the company in 2010, his primary responsibilities have included performing failure analysis investigations and providing metallurgical support for product and process development efforts. Prior to joining TimkenSteel, he earned a Bachelor's degree in materials science & engineering from the University of Connecticut.